Marine and Petroleum Geology 77 (2016) 435–447

Contents lists available at ScienceDirect

Marine and Petroleum Geology

journal homepage: www.elsevier.com/locate/marpetgeo

Research paper

Water-rock interaction and methanogenesis in formation water in the southeast Huaibei coalfield, China

Qingguang Li [a, b], Yiwen Ju [b, *], Weiqi Lu [c], Guochang Wang [b], Bhupati Neupane [b], Yue Sun [b]

[a] Environmental Science and Engineering Postdoctoral Research Center, School of Earth and Environment, Anhui University of Science and Technology, 232001, Huainan, China
[b] Key Lab of Computational Geodynamics of Chinese Academy of Sciences, College of Earth Science, University of Chinese Academy of Sciences, 100049, Beijing, China
[c] State Key Laboratory of Environmental Geochemistry, Institute of Geochemistry, Chinese Academy of Sciences, 550002, Guiyang, China

ARTICLE INFO

Article history:
Received 5 January 2016
Received in revised form
19 June 2016
Accepted 22 June 2016
Available online 29 June 2016

Keywords:
Water-rock interactions
End member discrimination
Methanogenesis
Microbial gas
Isotope geochemistry

ABSTRACT

The hydrogeochemical characteristics of aquifers in coal-bearing strata can provide an important foundation for understanding the evolution of the aquifers and recognizing the formation process and occurrence of biogenic gas. By analyzing the hydrogeochemical characteristics of water produced from the Cenozoic, the limestone, and the coal strata aquifers and the coalbed gas wells, this study focused on water-rock interactions and methanogenesis in the formation water of the Suzhou mining area, Huaibei coalfield, China. Tectonically, this is one of the most complex coalfields in China. The dissolution of evaporites, silicates, and carbonates controlled the chemical composition of the formation water. The Cenozoic aquifers have a relatively stable water quality type and balanced ionic composition, but more complex water-rock interactions occur in the coal strata and the limestone aquifers. Extensive methanogenic activity and methanogenesis could be recognized by the meteoric water recharge, positive $\delta^{13}C$ signatures for dissolved inorganic carbon (DIC; 15.4‰–26.2‰), lower sulfate concentrations (<2 mM), and higher levels of dissolved methane and DIC. The generation and enrichment of secondary biogenic gas in the coal seams was after the microbes' inoculation along with the freshwater infilling the fracture network.

1. Introduction

The prospective resource of coal-bed methane (CBM) in the Huaibei coalfield could reach 315.9 billion cubic meters (Jiang et al., 2010). As one of the CBM exploitation demonstration sites in China, the exploitation in the southeast of the coalfield has just started. Spatially, thermogenic gas, mixture gas, secondary biogenic gas, and a gas-weathered zone were distributed regularly from the bottom to the top and from the center to the margin of the cola-bearing sedimentary basin (Bao et al., 2014; Li et al., 2015). Considering that the hydrocarbon index ($C_{HC} = C_1/(C_2 + C_3)$) is much higher than 1000 and the $\delta^{13}C_{CH4}$ are partly lighter than −60‰, the study area should be very rich in secondary biogenic gas (Li et al., 2015).

Previous studies have shown that most of the microbial CBM in coal seams formed during later periods of coalification and developed in relationship to the injection of ancient meteoric water (McIntosh et al., 2002; Healy et al., 2011; Shuai et al., 2013; Pashin et al., 2014). Hence, researchers have paid greater attention to the generation mechanisms of microbial methane in ground water and their controlling factors (Scott et al., 1994; Aravena et al., 2003; Flores et al., 2008; Gao et al., 2013; Ju et al., 2014). To adequately understand the microbial activity and the formation process of microbial gas, it is necessary to analyze the chemical and isotopic compositions of related solutes in aquifers and the redox state of the water (Whiticar et al., 1986; Whiticar, 1999; Schlegel et al., 2011; Golding et al., 2013).

Moreover, the hydrogeochemical characteristics of the formation water may provide useful information about its evolutionary process, such as the degree of the water-rock interactions and the sources of the solutes (Négrel et al., 1993; Gaillardet et al., 1999; Yang et al., 2008; Li et al., 2014). Additionally, the water produced

* Corresponding author.
E-mail address: juyw03@163.com (Y. Ju).

http://dx.doi.org/10.1016/j.marpetgeo.2016.06.021
0264-8172/

during CBM exploitation may induce potential threats to surface water, soils, and ecosystems because of the higher salinity and heavy metal concentrations (Cheung et al., 2010; Healy et al., 2011; Yang et al., 2011). Thus, it is essential to research the geochemical features of the produced water and evaluate its influence on the environment surrounding the gas wells.

Based on the hydrogeological features of the study area and the long-term groundwater quality data, this study analyzed the associated chemical and isotopic compositions of the formation water and the produced water from CBM gas wells through systematic sampling. The aims are to (1) research the water-rock interactions and evolution process of the formation water and (2) evaluate the microbial activity and the formation pathway of microbial methane and its enrichment features.

2. Geological background

The Huaibei coalfield lies in northern Anhui Province (E: 115°58′–117°12′, N: 33°20′–34°28′), and its coal-bearing area is approximately 4100 km^2 (Jiang et al., 2010). Tectonically, this coalfield lies on the southeastern margin of the ancient North China Plate. Affected by the Dabie-Tanlu-Sulu orogenic evolution, the structural styles of the coalfield include linear tight folds and imbricate thrust faults (Wu et al., 2011). The main coal-bearing structures in the study area are the Sudong and the Sunan synclines (Fig. 1).

As one of the most geologically complex coalfields in China, the origin, occurrence, and distribution of CBM in the Huaibei coalfield differ in many ways from those coalfields with simple tectonic evolutions. Based on its tectonic-thermal-burial history, the process of CBM generation in the Huaibei coalfield occurred in three stages: (1) thermogenic gas generation, when the buried depth of coal seams increased rapidly; (2) gas escape, when the coal-bearing strata moved upward; and (3) the generation of secondary biogenic gas at a suitable temperature and burial depth (Wu et al., 2011).

2.1. Coal-bearing strata and gas content

The minable coal seams in this mining area mostly lie in the Permian strata (Table 1). The total thickness of the coal-bearing strata exceeds 1300 m, and the largest thickness for a single coal seam is 21 m (Zheng et al., 2008). According to Wu and Li (2005), the main coal seams have a relatively high gas content (6.9–25.5 m^3/t) and gas-bearing saturation (98%–100%).

2.2. Hydrogeology

The coal seams in the study area are all covered by unconsolidated Tertiary and Quaternary sediments. According to the lithology and the distribution of the aquifers, the formation water can be classified into three types (Table 1): the upper aquifers in the Cenozoic unconsolidated formations, the middle aquifers in the Permian coal strata, and the lower aquifers in the Carboniferous limestone strata (Gui, 2005; Chen et al., 2013a, 2013b).

2.2.1. Cenozoic aquifers

From north to south and east to west, the thickness of the Cenozoic sediments increases gradually and reaches hundreds of meters in the study area (Gui, 2005). Sand layers, gravel layers, and interlayers of claypan are the main components of these formations, and the hydraulic connections among the four aquifers in the Cenozoic formations are negligible because of the stable distribution and large thickness of the water-resistant interlayers.

The fifth aquifer, which lies in a Jurassic conglomerate layer, has a very high water-bearing capacity. However, this aquifer is controlled by paleotopography and exists only in shallow and marginal areas in the study area. Hence, the Cenozoic unconsolidated formations often directly overlie the coal-bearing strata.

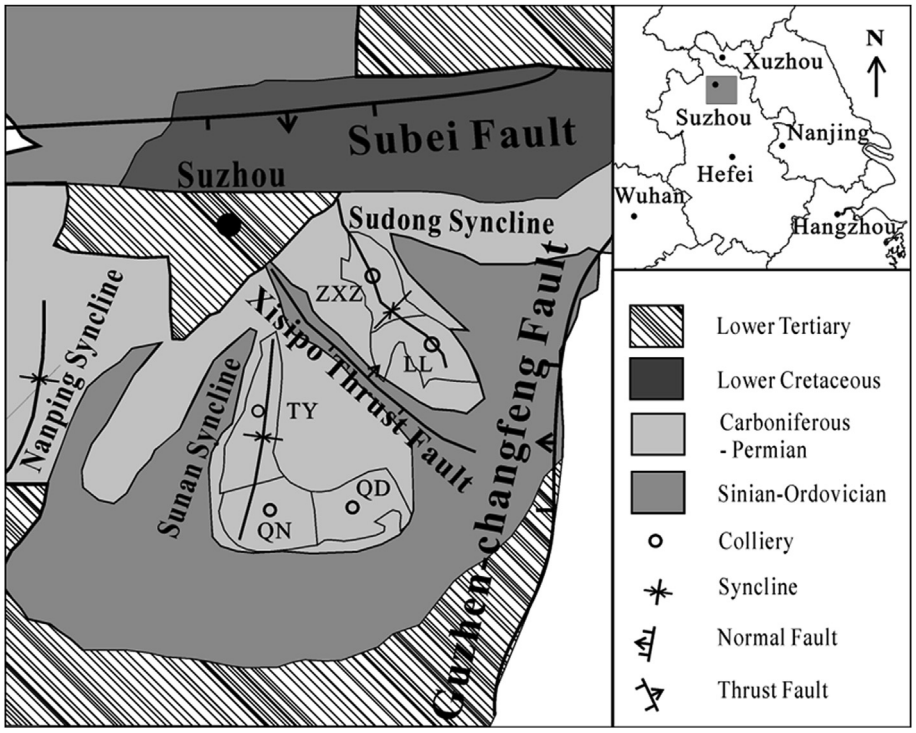

Fig. 1. Mining location and the main structure outline map (QD: Qidong colliery; QN: Qinan colliery; TY: Taoyuan colliery; ZXZ: Zhuxianzhuang colliery; LL: Lulling colliery).

Table 1
Strata and aquifers in the Suzhou mining area (modified from Gui, 2005).

Era	System	Formation	Lithology	Thickness (m)	Coal seam	Remarks
Cenozoic	Quaternary			126~303		No. 1, 2, and 3 aquifers
	Neogene			96~155		No. 4 aquifer
Mesozoic	Jurassic			0~240		Denudated and the No. 5 aquifer is at the bottom
Upper Paleozoic	Permian	Shiqianfeng		>544		Denudated and mostly lost
		Upper Shihezi			No.1-3	Sandstone fissure water, No. 6 aquifer
		Lower Shihezi				
	Carboniferous	Shanxi		256	No.4-9	No. 7 aquifer is between No. 7 and 10 coal seams
		Taiyuan		111	No.10	
		Benxi		150~170	Thin coal seams or coal lines	Limestone mixed withthin and unrecoverable coal seams or coal lines (No. 8 aquifer)
Lower Paleozoic	Ordovician			2~16		The product of an ancient weathering crust
						Marine carbonate deposits, composed of limestone (No. 9 aquifer)
	Cambrian					Oolitic limestone, dolomite limestone, siltstone and shale

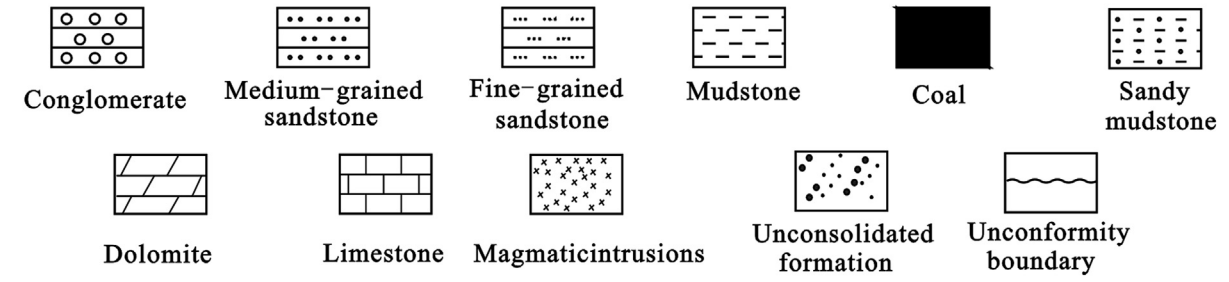

2.2.2. Coal strata aquifers

Coal strata aquifers are composed of sandstone and conglomerate. According to the vertical distribution of the strata, two aquifers can be distinguished (Table 1). The No. 6 aquifer lies between the third and the fourth coal seams, with an average thickness of approximately 90 m. The No. 7 aquifer lies between the seventh and the tenth coal seams, with an average thickness of approximately 70 m. The main petrographic composition of these two aquifers is fine-grained and medium-grained sandstone.

2.2.3. Limestone aquifers

The No. 8 and No. 9 aquifers lie in Carboniferous limestone strata. Though the carbonate content of the No. 8 aquifer accounts for only 40%, this is the aquifer that primarily threatens mine safety because of the shorter distance to the tenth coal seam (Gui, 2005). In contrast, due to the long distance, the threat of the No. 9 aquifer is lower despite its higher carbonate content and better water-bearing properties than those of the No. 8 aquifer.

3. Sampling and analytical methods

3.1. Sampling

The water produced from CBM wells and the formation water samples were collected from three collieries in the study area (QN: Qinan colliery; ZXZ: Zhuxianzhuang colliery; LL: Lulling colliery) in August 2013. All of the samples were filtered via glass fiber filter membranes and stored at 4 °C in a refrigerator before analysis. For cation and dissolved organic carbon (DOC) concentration tests, the samples were acidified to a pH of <3. For sterilization purposes, the saturated $HgCl_2$ solution was injected into the isotope analysis samples, including $\delta^{13}C$ of dissolved inorganic carbon (DIC), $\delta^{34}S$, and $\delta^{18}O$ of sulfate. In addition to sterilization, dissolved gas analysis samples were sealed bubble-free in serum bottles with rubber stoppers.

To comprehensively analyze the geochemical characteristics of different aquifers, a series of water quality data for the Cenozoic, the coal strata, and the limestone aquifers was collected from these three collieries (QN, LL, and ZXZ; Table 2) and published papers (Tables 3 and 4). With respect to data quality, data points with errors that exceed 5% were excluded during the cation-anionic equilibrium analysis.

3.2. Analytical methods

The bicarbonate concentration was titrated with a Metrohm automatic titration apparatus. The concentrations of Cl^-, SO_4^{2-}, and F^- were analyzed by ion chromatograph (Dionex−500). A PE-5100 atomic absorption spectrometer was used to analyze the concentrations of K^+, Na^+, Ca^{2+}, and Mg^{2+}. The total dissolved solids (TDS) was equivalent to the total mass concentration of the major ions (CO_3^{2-}, HCO_3^-, Cl^-, SO_4^{2-}, Ca^{2+}, Mg^{2+}, K^+, and Na^+) minus half of the bicarbonate concentration. The DOC concentration was tested with an Elementar High TOC analysis meter, and the pH was measured according to potentiometry. To form a headspace, 20 ml of high-purity nitrogen was injected into the dissolved gas sample to replace the same volume of water. After vibrating for 1 h at 20 °C, the headspace gas composition was analyzed by gas chromatography the next day to calculate the dissolved gas content.

The $\delta^{18}O$ and δD values of water were tested using a Finnigan MAT253 according to the TC/EA–IRMS method (Begley and Scrimgeour, 1997; Brenna et al., 1997). The results are expressed in the usual delta (δ) notation in ‰ deviation relative to Vienna Standard Mean Ocean Water (VSMOW). The accuracy is ±2‰ for δD and ±0.2‰ for $\delta^{18}O$, respectively. Samples for $\delta^{13}C$-DIC analysis were pretreated by injecting phosphoric acid to acquire CO_2 for testing. The acidified $\delta^{13}C$-DOC samples were freeze-dried, and CO_2 was acquired by DOC combustion in a sealed quartz tube. The instrument for $\delta^{13}C$ analysis was a Finnigan MAT253 with an analytical accuracy of ±0.2‰. The results for $\delta^{13}C$ are expressed in ‰ relative to the Vienna Pee Dee Belemnite (VPDB) standard.

Samples for $\delta^{34}S$-SO_4^{2-} and $\delta^{18}O$-SO_4^{2-} analysis had additions of HCl and $BaCl_2$ solutions to induce $BaSO_4$ precipitation. Then, SO_2 was produced in an elemental analyzer for $\delta^{34}S$ analysis (Cheung et al., 2010). The accuracy of the $\delta^{34}S$ analysis is ±0.2‰, and the results are expressed in ‰ relative to the Vienna Cañon Diablo Troilite (VCDT) standard. Values of $\delta^{18}O$ in sulfate were determined by testing CO_2 that was produced via a reduction reaction between sulfate and carbon powder. The accuracy of the $\delta^{18}O$ analysis is ±0.2‰, and the results are expressed in ‰ relative to the VSMOW standard. Both $\delta^{34}S$ and $\delta^{18}O$ of sulfate were analyzed by a Finnigan MAT253.

Table 2
Chemical composition of different aquifers obtained from three collieries (LL, ZXZ, and QN).

Location (amount)	pH min−max AVE±σ	Na^++K^+(mg/L) min−max AVE±σ	Mg^{2+}(mg/L) min−max AVE±σ	Ca^{2+}(mg/L) min−max AVE±σ	Cl^-(mg/L) min−max AVE±σ	SO_4^{2-}(mg/L) min−max AVE±σ	HCO_3^-(mg/L) min−max AVE±σ	TDS(mg/L) min−max AVE±σ
Cenozoic	7.10–8.60	5.5–742.4	35.8–330.6	21.6–464.9	17.9–378.5	36.2–2747.6	122.6–545.2	300–4241
aquifer(66)	7.72 ± 0.30	279.3 ± 103.4	92.3 ± 51.9	151.6 ± 75.3	280.0 ± 93.8	616.5 ± 432.4	384.7 ± 68.1	1612 ± 529
Limestone	7.06–8.63	151.8–483.3	4.8–112.0	10.3–251.2	106.8–347.5	8.2–865.9	358.1–793.8	958–1948
aquifer(49)	7.55 ± 0.42	261.2 ± 69.7	72.0 ± 32.1	141.4 ± 76.5	240.7 ± 51.6	488.0 ± 226.0	453.8 ± 75.8	1430 ± 312
Coal strata	7.24–10.33	202.5–1173.6	2.2–403.9	1.2–289.0	67.9–371.5	1.7–2590.2	290.5–3021.4	543–3892
aquifer (59)	8.34 ± 0.60	447.6 ± 171.2	29.9 ± 73.3	33.6 ± 68.3	190.1 ± 106.8	304.5 ± 626.8	654.0 ± 413.4	1237 ± 619
Produced	8.15–8.45	1453.6–2628.9	4.9–12.5	3.8–22.7	249.0–680.0	1.0–21.9	2426.0–5400.0	3400–6028
water(9)	8.30	1917.3 ± 441.0	8.5 ± 2.7	13.2 ± 5.6	456.8 ± 175.6	5.9 ± 7.4	3812.3 ± 984.2	4397 ± 982

Table 3
Chemical composition and isotope data of formation water in the Suzhou mining area (from Chen et al., 2013a). TDS* is equivalent to the total mass concentration of the major ions after subtracting half of the bicarbonate concentration.

NO.	Colliery	Seam	K^++Na^+ (mg/L)	Mg^{2+}(mg/L)	Ca^{2+}(mg/L)	Cl^-(mg/L)	SO_4^{2-}(mg/L)	HCO_3^-(mg/L)	CO_3^{2-}(mg/L)	$\delta^{13}C$–DIC (‰/VPDB)	$\delta^{34}S$–SO_4^{2-} (‰/CDT)	TDS* (mg/L)
23	ZXZ	Cenozoic aquifer	371.7	55.8	58.7	199.1	426.4	560.2	0.0	−5.5	26.2	1391.8
24	ZXZ	Cenozoic aquifer	354.5	74.4	82.4	269.3	421.9	565.2	0.0	−9.2	26.2	1485.1
25	ZXZ	Cenozoic aquifer	354.5	48.1	49	329	161.4	661.3	0.0	−11.2	26.7	1272.65
32	TY	Cenozoic aquifer	136.0	74.9	186.8	301.3	212.3	488.2	0.0			1155.4
33	QD	Cenozoic aquifer	308.1	82.7	111.9	223.2	586.1	444.2	0.0	−8.3	26.8	1534.1
82	ZXZ	Coal strata aquifer	564.6	10.4	32.6	360.4	208.3	764.4	0.0	−12.6	25.6	1558.5
83	ZXZ	Coal strata aquifer	548.0	10.1	15.2	362.6	14.4	908.6	0.0	−13.9		1404.6
84	ZXZ	Coal strata aquifer	540.7	11.1	26.7	355.4	164.6	750.6	0.0	−10.8	26.1	1473.8
85	ZXZ	Coal strata aquifer	603.3	9.4	11.7	364.4	14.8	1037.6	0.0	−11.6		1522.4
86	ZXZ	Coal strata aquifer	483.4	9.6	12.1	371.5	205.4	467.1	0.0	−8.0	26.2	1315.6
88	LL	Coal strata aquifer	727.2	1.9	1.6	164.8	29.2	1252.2	178.1			1728.9
102	QD	Coal strata aquifer	655.9	3.6	4.2	197.2	14.8	1151.1	128.6	15.4	23.6	1579.9
151	LL	Limestone aquifer	185.5	40.6	55.9	92.5	139.9	529.1	0.0	−8.2	26.3	779.0
153	LL	Limestone aquifer	173.3	43.1	63.6	99.4	149.8	508.1	0.0	−7.2	25.7	783.3
155	QN	Limestone aquifer	27.3	93.8	190.8	251.7	220	405.8	0.0			986.5

Table 4
Results of TDS, $\delta^{18}O-H_2O$, and $\delta D-H_2O$ in the Suzhou mining area.

Colliery	Seam	$\delta^{18}O-H_2O$ (‰)	$\delta D-H_2O$ (‰)	TDS (mg/L)	Reference
QN	Coal strata aquifer	−8.8	−77.2	1050	Chen et al., 2013b
ZXZ	Coal strata aquifer	−9.3	−64.5	1599	Chen et al., 2013b
ZXZ	Coal strata aquifer	−8.6	−63.3	1446	Chen et al., 2013b
ZXZ	Coal strata aquifer	−7.8	−61.1	1517	Chen et al., 2013b
ZXZ	Coal strata aquifer	−7.4	−61.3	1570	Chen et al., 2013b
ZXZ	Coal strata aquifer	−8.2	−63.0	1354	Chen et al., 2013b
QD	Coal strata aquifer	−8.6	−63.1	1613	Chen et al., 2013b
TY	Cenozoic aquifer	−9.3	−70.3	1155	Gui, 2005
ZXZ	Cenozoic aquifer	−7.9	−75.1	393	Gui, 2005
LL	Cenozoic aquifer	−8.9	−72.5	555	Gui, 2005
ZXZ	Cenozoic aquifer	−8.4	−64.3	1429	Chen et al., 2013b
ZXZ	Cenozoic aquifer	−8.0	−62.3	1521	Chen et al., 2013b
ZXZ	Cenozoic aquifer	−8.1	−61.5	1469	Chen et al., 2013b
ZXZ	Cenozoic aquifer	−6.7	−52.3	241	Chen et al., 2013b
ZXZ	Cenozoic aquifer	−7.3	−58.2	220	Chen et al., 2013b
ZXZ	Cenozoic aquifer	−7.8	−57.9	375	Chen et al., 2013b
ZXZ	Cenozoic aquifer	−7.1	−53.9	350	Chen et al., 2013b
TY	Cenozoic aquifer	−9.3	−70.3	1155	Chen et al., 2013b
QD	Cenozoic aquifer	−8.5	−62.7	1579	Chen et al., 2013b
TY	Limestone aquifer	−8.8	−61.4	1005	Gui, 2005
QN	Limestone aquifer	−5.5	−69.0		Gui, 2005
QN	Limestone aquifer	−8.5	−70.1	986	Gui, 2005
ZXZ	Limestone aquifer	−7.5	−63.6	243	Gui, 2005
LL	Limestone aquifer	−8.0	−59.4	539	Chen et al., 2013b
LL	Limestone aquifer	−6.7	−44.3	317	Chen et al., 2013b
LL	Limestone aquifer	−8.0	−59.9	809	Chen et al., 2013b
TY	Limestone aquifer	−8.8	−61.4	1005	Chen et al., 2013b
QN	Limestone aquifer	−8.5	−70.1	986	Chen et al., 2013b

During the isotope testing, we had one international standard and two national standards for $\delta^{18}O$, δD, $\delta^{13}C$, and $\delta^{34}S$ standard calibration (Table 5). Based on the linear regression equation of the truth-value and the measured value of the three standards correspondingly, the measured isotope compositions of the samples were normalized (Coplen, 2011).

4. Results

The results of the major ions and isotopes are summarized in Table 6 A and B. On the whole, the Cenozoic and the limestone aquifers have similar pH values, with average values of 7.72 and 7.55, respectively, while the coal strata aquifer values are much higher (8.34 on average). The TDS values in the three types of aquifers are similar and less than 2000 mg/L, but reach 4397 mg/L on average in the produced water. This is higher than another CBM demonstration area (2854 mg/L in average) in Liulin, Shanxi Province (Yang et al., 2011). The average TDS of the produced water in the Powder River Basin is only 862 mg/L (Rice et al., 2000).

Table 5
The truth and measured values of different standards.

	Standard name	Truth−value (‰)	Measured value (‰)
δD	GBW04401	−0.40	−0.51
	GBW04402	−68.80	−64.91
	GISP	−189.50	−188.11
$\delta^{18}O$	GBW04401	0.32	0.40
	GBW04402	−8.79	−8.71
	GISP	−24.80	−24.52
$\delta^{13}C$	NBS−18	−5.01	−5.02
	GBW04407	−22.43	−22.35
	GBW04408	−36.91	−36.71
$\delta^{32}S$	NBS−123	17.10	17.01
	GBW04414	−0.07	−0.10
	GBW04415	22.15	22.02

The average total cation contents ($TZ^+ = Na^+ + K^+ + Mg^{2+} + Ca^{2+}$) of the Cenozoic, the coal strata, and the limestone aquifers are 26.4, 23.0, and 22.0 meq/L, respectively (Table 7). These values are obviously higher than global surface/river water averages (TZ^+: 0.3–10.0 meq/L; Meybeck, 1981). Moreover, the produced water has an even higher total cation content (TZ^+ = 76.0 meq/L on average). Na^+ and K^+ are the main cations of the three types of aquifers. Especially in the coal strata aquifers and the produced water, Na^+ and K^+ are much higher, exceeding 90% of the total cation content. The major anion is HCO_3^-, followed by Cl^- and SO_4^{2-}, in all three types of aquifers. However, the predominance of HCO_3^- is not obvious in the Cenozoic aquifers. Additionally, the content of SO_4^{2-} decreases in the following order: the Cenozoic and limestone aquifers, the coal strata aquifers, and the produced water.

The desulfurization coefficients ($\gamma_{SO4}/[\gamma_{SO4}+\gamma_{Cl}]$) of the Cenozoic and the limestone aquifers are greater than 30%, but the coefficient is lower than 0.6% in produced water (Table 7). The γ_{Na}/γ_{Cl} coefficients all exceed 1.0 in the three types of aquifers. In the produced water, the value even reaches an average of 6.5. Additionally, though the dissolved gas concentration has a large range (36.1–1238.8 μl/L), samples collected from the produced water have stable values greater than 700 μl/L.

The δD and $\delta^{18}O$ values of the groundwater in the Cenozoic aquifers are characterized by a δD range between −52.3‰ and −75.1‰ and a $\delta^{18}O$ range between −6.7‰ and −9.3‰ (Table 6B). For the limestone aquifers, the δD range is −44.3‰ to −70.1‰ and the $\delta^{18}O$ range is −5.5‰ to −8.8‰. For the coal strata aquifers, the δD range is −55.2‰ to −77.2‰ and the $\delta^{18}O$ range is −7.4‰ to −9.3‰. For the produced water, the δD and $\delta^{18}O$ ranges are −56.9‰ to −61.0‰ and −8.4‰ to −8.9‰, respectively.

The $\delta^{13}C_{DIC}$ values can be divided into two groups (Table 6B). One group includes more positive isotopic compositions from 20.6‰ to 26.2‰, and the other group includes more negative isotopic compositions from −9.4‰ to −1.1‰. Overall, there appears to be no obvious $\delta^{13}C_{DOC}$ differences among different aquifers

Table 6A
Chemical and isotopic composition of water samples collected from the Suzhou mining area. TDS* is equivalent to the total mass concentration of the major ions after subtracting half of the bicarbonate concentration.

Sample NO.	Aquifer	pH	Na^+ (mg/L)	K^+ (mg/L)	Mg^{2+} (mg/L)	Ca^{2+} (mg/L)	F^- (mg/L)	Cl^- (mg/L)	SO_4^{2-} (mg/L)	HCO_3^- (mg/L)	CO_3^{2-} (mg/L)	Br^- (mg/L)	TDS* (mg/L)
14	Cenozoic aquifer	7.12	272.0	42.7	93.9	388.0	1.2	316.0	1060.0	463.0		0.6	2361.4
1	Limestone aquifer	7.60	189.0	5.6	34.9	71.4	1.0	85.5	161.0	555.0		0.1	819.3
2	Limestone aquifer	7.61	541.0	2.6	1.7	7.1	4.3	115.0	46.7	1178.0		0.4	1300.5
3	Limestone aquifer	7.58	201.0	4.2	29.8	54.5	0.5	84.2	149.0	560.0		0.2	798.5
15	Coal strata aquifer	7.67	590.0	4.0	2.4	9.7	0.6	334.0	18.9	1013.0		0.6	1461.5
13	Coal strata aquifer	8.34	1235.0	22.1	2.1	11.2	2.6	924.0		1264.0	167.0	2.5	2971.3
4	Produced water	8.39	1809.0	37.3	4.9	22.7	2.1	249.0	4.3	4234.0	217.0	0.9	4423.9
5	Produced water	8.29	2244.0	65.7	12.5	3.8	1.2	628.0		4434.0	182.0	1.6	5287.3
6	Produced water	8.45	1585.0	26.1	7.1	20.7	2.4	258.0	1.5	3247.0	255.0	0.9	3750.8
7	Produced water	8.15	2417.0	59.1	5.7	10.0	2.2	492.0	2.1	5400.0		1.2	5626.8
8	Produced water	8.31	2574.0	54.9	9.3	13.3	1.1	680.0	1.0	4807.0	347.0	1.2	6028.1
9	Produced water	8.19	1721.0	33.9	6.5	13.3	1.8	390.0	7.2	3830.0		0.8	4053.0
10	Produced water	8.35	1689.0	11.7	12.5	12.6	1.3	525.0	3.1	2998.0	238.0	0.4	3979.2
11	Produced water	8.30	1466.0	8.6	9.5	12.0	2.8	637.0		2426.0	189.0	0.5	3526.5
12	Produced water	8.31	1440.0	13.6	8.8	10.8	1.9	252.0	21.9	2935.0	199.0	0.7	3400.0

Table 6B
Chemical and isotopic composition of water samples collected from the Suzhou mining area. TDS* is equivalent to the total mass concentration of the major ions after subtracting half of the bicarbonate concentration.

Sample NO.	Seam	CH_4 (μl/L)	TOC (mg/L)	$\delta D-H_2O$ (‰/VSMOW)	$\delta^{18}O-H_2O$ (‰/VSMOW)	$\delta^{13}C-DIC$ (‰/VPDB)	$\delta^{34}S-SO_4^{2-}$ (‰/CDT)	$\delta^{18}O-SO_4^{2-}$ (‰/SMOW)	$\delta^{13}C-DOC$ (‰/VPDB)
14	Cenozoic aquifer	/	1.0	−61.3	−8.6	−1.1	28.5	14.4	−24.4
1	Limestone aquifer	/	1.3	−59.0	−8.2	−8.9	22.4	22.1	−21.3
2	Limestone aquifer	36.1	1.6	−58.8	−8.4	−7.6	25.0	22.7	−26.6
3	Limestone aquifer	386.4	1.2	−58.5	−8.0	−3.1	20.8	19.0	−25.4
15	Coal strata aquifer	108.3	0.8	−62.2	−8.8	−9.4	29.8	12.3	−25.5
13	Coal strata aquifer	816.7	1.1	−53.6	−8.0	20.4	12.9		−25.2
4	Produced water	737.0	1.5	−58.3	−8.8	21.1	16.1	23.7	−25.4
5	Produced water	725.1	1.3	−57.1	−8.6	25.7	16.0	18.7	−22.3
6	Produced water	753.8	1.7	−58.5	−8.6	24.9	17.5		−27.0
7	Produced water	773.9	0.9	−57.7	−8.5	26.0	17.2	11.2	−21.8
8	Produced water	1238.8	0.7	−55.3	−8.5	25.8	15.6	0.1	−25.1
9	Produced water	777.5	1.3	−57.4	−8.5	25.0	17.2	9.0	−24.2
10	Produced water	841.4	1.2	−57.4	−8.4	22.8	18.2		−25.7
11	Produced water	873.8	1.0	−57.1	−8.3	22.6	15.6		−26.4
12	Produced water	891.1	1.4	−59.4	−8.6	23.5	17.0	13.4	−25.5

Table 7
Parameters of different aquifers calculated according to Tables 2 and 5

Location (amount)	TZ^+(meq/L) min–max AVE	γ_{Na}/γ_{Cl} min–max AVE	$(Mg^{2+}+Ca^{2+})/HCO_3^-$ min–max AVE	Mg^{2+}/Ca^{2+} min–max AVE	$\gamma_{SO4}/\gamma_{SO4+Cl}$ min–max AVE	$[Na^++K^+]/[Ca^{2+}+Mg^{2+}]$ min–max Molar ratio
Cenozoic aquifer (66)	6.1–64.9	0.2–17	0.8–13.4	0.4–3.4	13%–72.9%	0–4.7
	26.4	1.9	2.6	1.2	39.9%	1.7
Limestone aquifer(49)	13.0–28.1	0.9–3.3	0.1–3.1	0.5–2.0	24.1%–94.3%	0.6–13.8
	23	1.7	1.9	1.0	42.9%	3.5
Coal strata aquifer(59)	9.9–63.7	1.6–17.0	0.02–9.65	0.4–6.1	0.6%–94.3%	2.3–225.9
	22	4.5	0.6	1.8	24.8%	40.3
Produced water(9)	58.2–103.7	3.3–10.3	0.01–0.02	0.4–5.5	0.0–3.1%	78.0–198.3
	76	6.5	0.01	1.5	0.6%	114.3

(−21.7‰ to −27.4‰). Both the $\delta^{34}S-SO_4^{2-}$ and $\delta^{18}O-SO_4^{2-}$ compositions are characterized by positive values and large ranges (13.0‰–30.0‰ for $\delta^{34}S-SO_4^{2-}$, 9.0‰–23.8‰ for $\delta^{18}O-SO_4^{2-}$). Due to low concentrations, the $\delta^{18}O-SO_4^{2-}$ compositions of several samples were not analyzed.

5. Discussion

According to Figs. 2 and 3, the Cenozoic aquifers have a relatively stable and balanced ionic composition, and the water is basically of the Na–Ca–Mg–SO_4–Cl–HCO_3 type. However, there

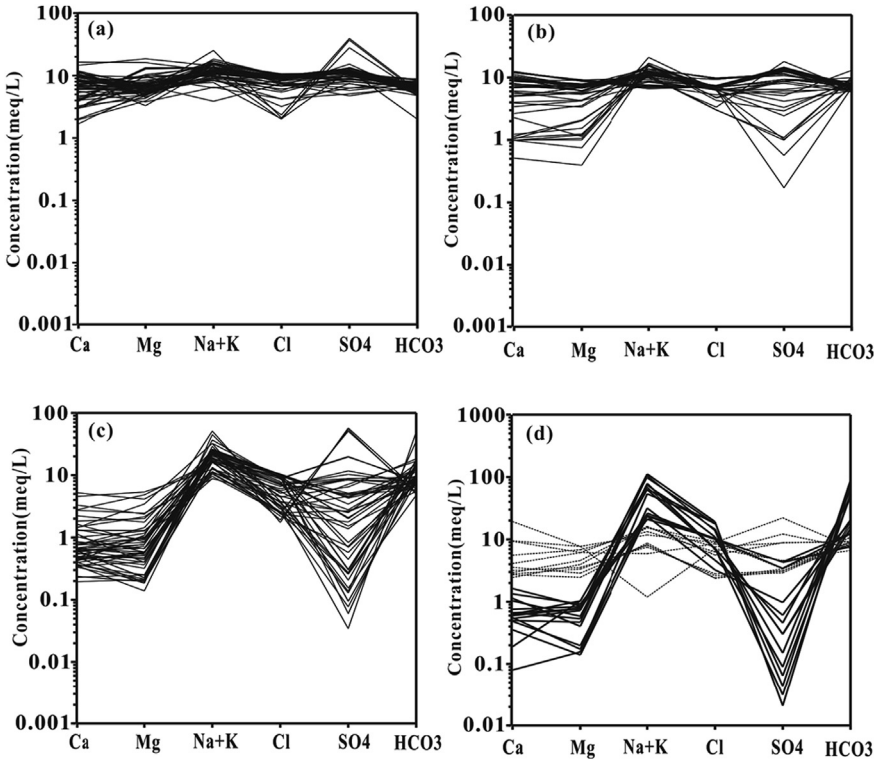

Fig. 2. Schoeller diagrams illustrating the chemical composition of (a) Cenozoic aquifer; (b) Limestone aquifer; (c) Coal strata aquifer; (d) Samples collected in this study—the bold lines represent produced water samples and the fine lines represent samples collected from collieries.

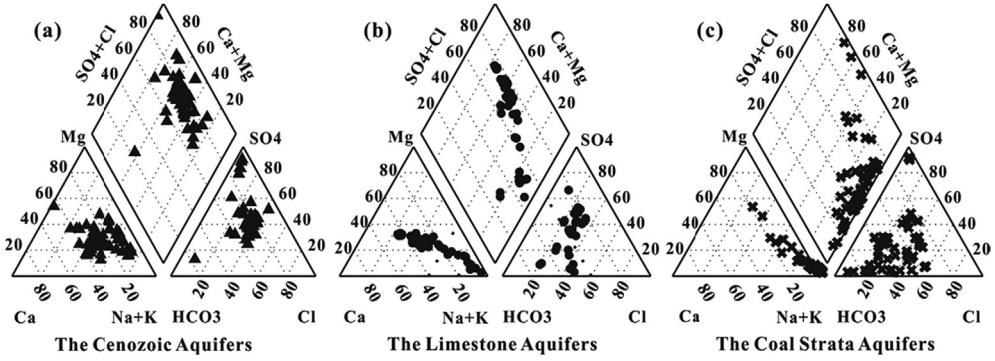

Fig. 3. Piper diagrams illustrating the chemical composition of the (a) Cenozoic aquifers; (b) Limestone aquifers; (c) Coal strata aquifers.

are two obviously different water quality types in the limestone aquifers: Na–Ca–Mg–SO4–Cl–HCO3 and Na–HCO3–Cl.

In the coal strata aquifers, the concentrations of Ca^{2+} and Mg^{2+} are generally lower than those in the Cenozoic and limestone aquifers, and the SO_4^{2-} concentrations feature a larger range. Though the chemical composition is more complicated than that in the Cenozoic and limestone aquifers (Figs. 2 and 3), most of the samples from the coal strata aquifers are of the Na–HCO_3–Cl type. Moreover, the ionic composition of the produced water is a very stable Na–HCO_3 type.

5.1. Water-rock interaction

In the sealed condition, the Mg/Ca molar ratio of the formation water is mainly controlled by water-rock interactions. At room temperature, the Mg/Ca ratio should be approximately 0.8 if the interaction between water and minerals such as calcite and dolomite is balanced (Appelo and Postma, 2005; Han and Liu, 2005), and this ratio decreases along with the increasing temperature. Moreover, the precipitation of calcite might induce the relative enrichment of Mg^{2+} (McIntosh et al., 2002). The Mg/Ca ratios of the three types of aquifers are all greater than 1.0, which demonstrates the relative enrichment of Mg^{2+}. Hence, during the evolution of groundwater, a certain degree of calcite precipitation might occur in appropriate areas.

In the coal strata aquifers, the $[Mg^{2+}+Ca^{2+}]/[HCO_3^-]$ ratio is just 0.6 on average. The extra HCO_3^- might originate from the dissolution of CO_2 generated during the breakdown of organic matter caused by thermal degradation and/or biodegradation. The higher HCO_3^- concentration (>1000 mg/L) could also promote calcite precipitation (Table 2). Additionally, the lower Mg^{2+} and Ca^{2+} concentrations among the three types of aquifers may also reflect the same process in the coal strata aquifers.

There are abundant Mg^{2+} and Ca^{2+} ions in the Cenozoic and the

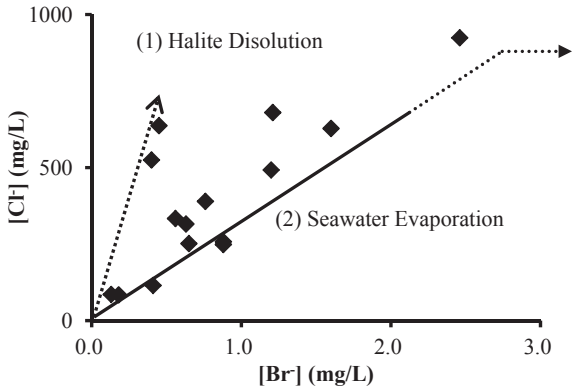

Fig. 4. [Cl^-] vs [Br^-] relation for coal strata aquifers according to Table 2a; halite dissolved in pure water produces the trajectory shown by arrow 1, and seawater evaporation short of halite precipitation is shown by arrow 2 (based on Martini et al., 1998).

limestone aquifers because the [Mg^{2+}+Ca^{2+}]/[HCO_3^-] ratios exceed 1.0. This is likely related to the dissolution of sulfate minerals such as gypsum, which is also supported by the higher SO_4^{2-} concentrations. The HCO_3^- concentration is the lowest in the Cenozoic aquifers, which is only 58% of that in the coal strata aquifers on average. One possible reason for this might be the lack of additional CO_2 sources as compared to the coal strata aquifers.

Considering the low Cl^- concentration in the meteoric water, its contribution to the solutes in these three types of aquifers appears to be negligible. The relatively high Cl^- concentration in the formation water seems to be caused by halite dissolution, according to Fig. 4, because the Cl^-/Br^- ratio in seawater is usually approximately 300 and the Cl^- concentration would increase noticeably during evaporite dissolution (Martini et al., 1998; McIntosh et al., 2002; Zhang et al., 2009).

The average ratios of [Na^++K^+]/[Ca^{2+}+Mg^{2+}] in the coal strata aquifers and the produced water exceed 40 (Table 7). The evaporite dissolution might be another reason for such high [Na^++K^+]/[Ca^{2+}+Mg^{2+}] ratios apart from ion exchanges (Brinck et al., 2008). When the sodium-adsorption ratio (SAR = [Na^+]/[Ca^{2+}+Mg^{2+}]) in the formation water exceeds 13, the direct discharge of this type of water would damage the soil structure because of the sodium replacement of calcium and magnesium (Healy et al., 2011; Yang et al., 2011). Hence, it would be undesirable for the direct discharge of the formation water from the coal and CBM exploration in the study area.

5.1.1. End member discrimination

When the coal-bearing strata lifted to the near-surface depth, the main controlling factors for carbonate dissolution became sulfuric acid and carbonic acid in the oxidative weathering condition (Han and Liu, 2005):

$$3Ca_xMg_{(1-x)}CO_3 + H_2CO_3 + H_2SO_4 = 3xCa^{2+} + 3(1-x)Mg^{2+} + 4HCO_3^- + SO_4^{2-}$$

Thus, a considerable amount of Mg^{2+} and Ca^{2+} is used to balance the SO_4^{2-} originating from the dissolution of sulfate-bearing minerals, such as gypsum. The remaining Mg^{2+} and Ca^{2+} ions ([Ca^{2+}+ Mg^{2+}]* = [Ca^{2+}+Mg^{2+}]–[SO_4^{2-}]) are mainly used to balance HCO_3^- and reflect the carbonate dissolution. Similarly, a certain amount of Na^+ and K^+ is used to balance Cl^-, which might be related to evaporite dissolution. Accordingly, the remaining Na^+ and K^+ ions ([Na^++ K^+]* = [Na^++ K^+]–[Cl^-]) are possibly related to silicate dissolution. Hence, the [HCO_3^-]-normalized [Na^++K^+]* and [Ca^{2+}+Mg^{2+}]* concentrations could reflect the relative contribution of silicates and calcites.

In the coal strata aquifers, silicate dissolution is the main end member (Fig. 5). A small portion of the data is beyond the silicate end member, which indicates that extra Na^+ and K^+ are needed to balance SO_4^{2-}. This might be related to the dissolution of minerals such as mirabilite. The Cenozoic and the limestone aquifers seem to have similar contributions of carbonates and silicates.

The ratios of different ions are useful parameters that could reflect different end member compositions in the formation water (Négrel et al., 1993; Gaillardet et al., 1999; Appelo and Postma, 2005). For example, the Na-normalized ratios of [HCO_3^-], [Mg^{2+}], and [Ca^{2+}] can effectively demonstrate end member compositions such as evaporites, carbonates, and silicates (Fig. 6). The contribution of evaporites seems to be the largest in all these three kinds of aquifers. Moreover, the carbonate end member contributes less in coal strata aquifers, which meshes well with the insights Fig. 5 offers. The data from the Cenozoic and the limestone aquifers are mostly located around the silicate end member in Fig. 6a and b, but this does not mean silicates contribute most of the solutes. Considering that this end member lies between evaporite and silicate end members, the contributions of these two end members should not be ignored.

On the whole, the dissolution of evaporites, silicates, and carbonates controls the chemical composition of the formation water. In the coal strata aquifers, evaporites and silicates contribute most of the solutes, and carbonates contribute less. In the Cenozoic and limestone aquifers, carbonates and silicates make similar contributions, but the contribution of evaporites seems to be larger.

5.2. Methanogenesis in the formation water

Previous research has shown that methanogens are very

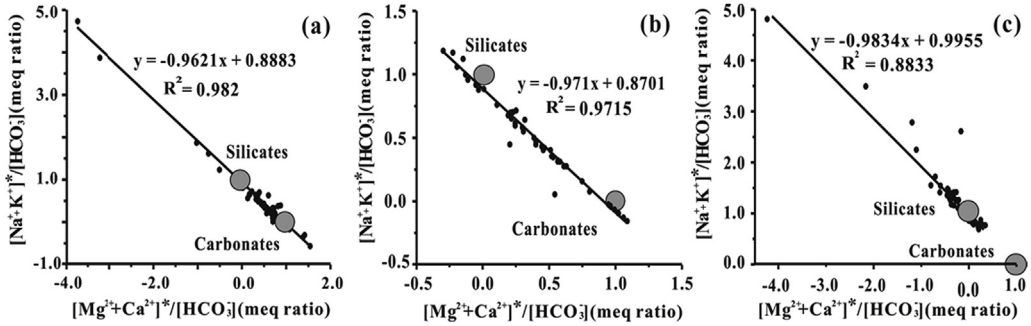

Fig. 5. Relationships of [Na^++K^+]* vs [Ca^{2+}+Mg^{2+}]* normalized by [HCO_3^-] ([Na^++K^+]* = [Na^++K^+]–[Cl^-]; [Ca^{2+}+Mg^{2+}]* = [Ca^{2+}+Mg^{2+}]–[SO_4^{2-}]) (a: Cenozoic aquifers; b: Limestone aquifers; c: Coal strata aquifers; after Han and Liu, 2005).

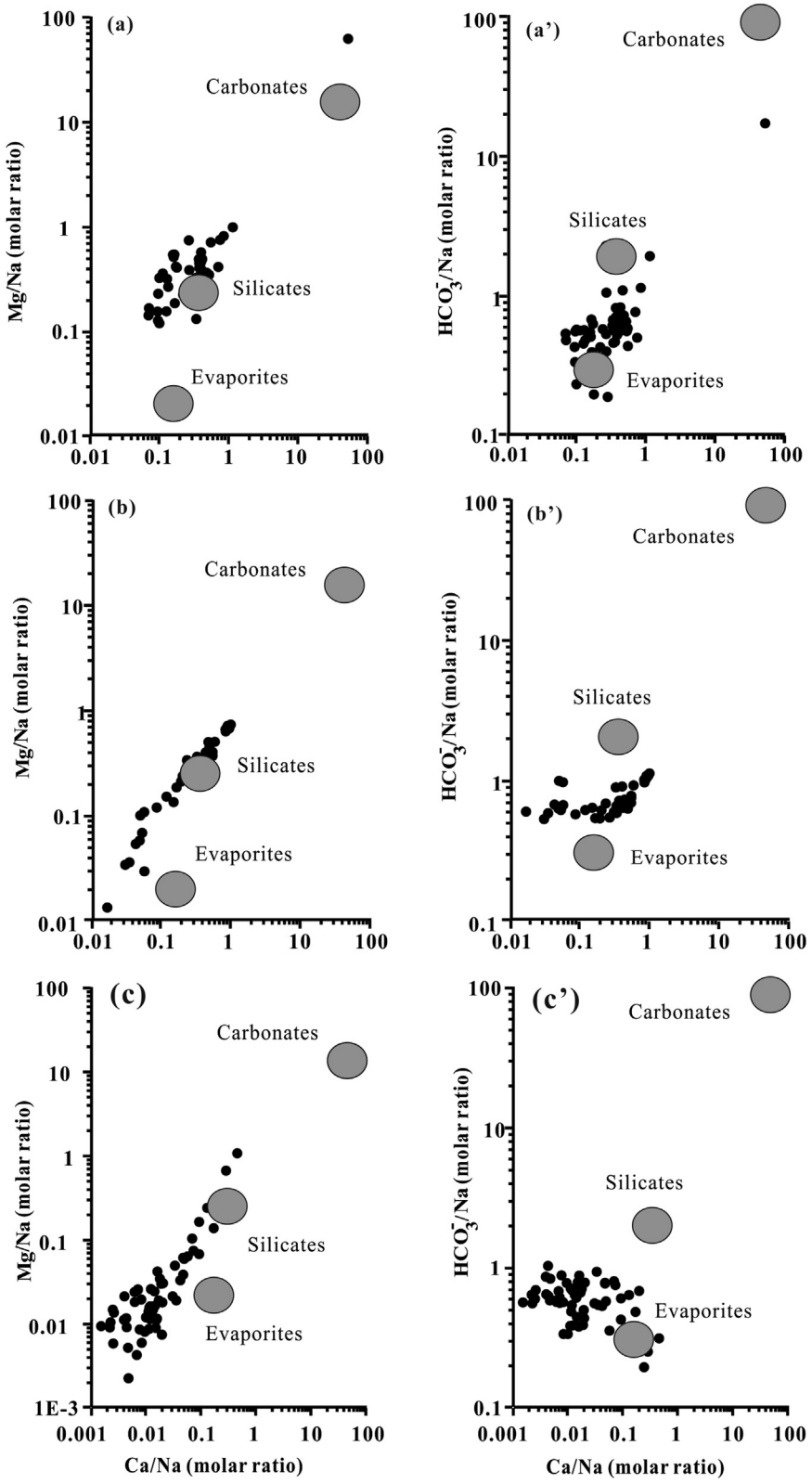

Fig. 6. Diagrams for determination of the end member compositions by HCO_3/Na vs. Ca/Na (a, b, c) and Mg/Na vs. Ca/Na (a', b', c') molar ratios (a and a': Cenozoic aquifers; b and b': Limestone aquifers; c and c': Coal strata aquifers) (based on Gaillardet et al., 1999; Xu and Liu, 2010).

sensitive to high levels of nitrate and high oxygen partial pressure (Whiticar, 1999). The rapid reproduction of methanogens occurs only in an anoxic environment (Eh < 200 mV) with appropriate pH ranges (4.0 < pH < 9.0; Schlegel et al., 2011). Due to the competitive advantage of the sulfate-reducing bacteria (SRB), stronger sulfate reduction would weaken the metabolism of methanogens when the sulfate concentration exceeds 10 mM (Rice and Claypool, 1981; McIntosh and Martini, 2008; Mitterer, 2010). Additionally, high

salinity would also affect the survival of methanogens (Zinder, 1993; Martini et al., 1998).

Although the high TDS levels would restrict the methanogen activity and the generation of microbial methane, methanogenesis has been shown to remain active under TDS conditions exceeding 70,000 mg/L in Alberta, Canada, and Louisiana, USA (Warwick et al., 2008; Cheung et al., 2010). Considering that the highest TDS value is only 6028 mg/L in the study area, it is much lower and more favorable for methanogens. In addition, the pH of the coal strata aquifers (8.34 in average) is also favorable for methanogens.

5.2.1. Evidence from meteoric water recharge

According to previous studies, microbial CBM is often related to meteoric recharge (McIntosh et al., 2002; Gao et al., 2013; Zhang et al., 2013; Pashin et al., 2014). Tectonic evolution in the study area was very intense, and the coal-bearing strata were uplifted to near-surface depth around 65 Ma (Wu et al., 2011). After the Miocene, the coal-bearing strata became stable, and the burial depth was less than 1000 m. This is very likely to provide favorable conditions for meteoric water recharge. In addition, the ground temperature (27–50 °C) during this time was also favorable for the reproduction of methanogens (Scott et al., 1994; Wu et al., 2011).

Fig. 7 shows the δD and $\delta^{18}O$ data for different aquifers in the study area. The intersection of the local meteoric water line (LMWL) and the local evaporation line (LEL; $\delta^{18}O$: −7.8‰; δD: −53.0‰) reflects the average isotopic composition of the local meteoric water. Most of the data points are all below the LMWL and have lighter isotopic compositions than the average value of local meteoric water. This is possibly related to the cold climate when ancient meteoric water recharged the formation water (Stueber and Walter, 1994; Weaver et al., 1995; Martini et al., 1998; Rice et al., 2008). In the Cenozoic aquifers, the regression line is sub-parallel to the LMWL; researchers have observed this phenomenon in several studies (Chapman et al., 2003; Huang et al., 2013). Their explanation for this is that the precipitation from different air masses with different isotopic compositions condensed in a dry climate, but no isotope fractionation occurred during transpiration.

Interestingly, some of the data points from the coal strata aquifers are located to the right of the LMWL. Evaporation, water-rock interaction, and mixing with basinal brines are all likely to be the reason for this (Golding et al., 2013; Hamilton et al., 2014). Considering that the regression line for these data has a lower slope than that of the LEL, water-rock interaction and mixing with basinal brines are left to be the possible reasons. Moreover, the $\delta^{18}O$ values are more negative along with lower Cl^- concentrations (Fig. 8). This could confirm the mixture of formation water and ancient meteoric water (Martini et al., 1998; McIntosh and Martini, 2008). Additionally, certain produced water data points located above the LMWL in Fig. 7 might indicate extensive isotopic fractionation induced by intense methanogenic activity (Rice et al., 2008).

5.2.2. Evidence from sulfate

The main sources of sulfate include the dissolution of minerals, such as gypsum and mirabilite, and sulfide oxidation. The increasing SO_4^{2-}concentration pattern relative to Cl^- is likely related to the dissolution of sulfate minerals (Fig. 9a). However, there appears to be no evidence for the oxidation of sulfides according to sulfate isotope features (Fig. 10). Hence, the dissolution of related minerals in a reducing environment should be the main source of sulfate for the coal strata aquifers. The reducing condition is also favorable for methanogenesis.

When the sulfate reduction reaction is strong, $\delta^{34}S\text{-}SO_4^{2-}$ would have a negative relation with SO_4^{2-} concentrations. Hence, the positive correlation between $\delta^{34}S\text{-}SO_4^{2-}$ and SO_4^{2-} concentrations possibly reflects that the sulfate reduction reaction is not obvious (Fig. 9b). Accordingly, the SRB activity would be greatly limited in aquifers with low SO_4^{2-} concentrations (<500 mg/L; Van Voast, 2003). In the study area, more than two-thirds of the SO_4^{2-} concentrations in the coal strata aquifers fall below 200 mg/L (Table 3). Strong sulfate reduction might have occurred in the early stage of the aquifers' evolution, but the low SO_4^{2-} concentrations restricted SRB activity soon afterward. This is favorable for the reproduction of methanogens and the generation of biogenic gas (McIntosh et al., 2002; Van Voast, 2003; Warwick et al., 2008; Mitterer, 2010).

5.2.3. Evidence from DIC, DOC, and dissolved gas

According to the analysis of water-rock interactions, the dissolution of CO_2 is the main reason for the high DIC content in the coal strata aquifers. CO_2 generated from the thermal degradation of organic matter should have $\delta^{13}C$ values (−22‰ to −27‰) similar to those found in the coal (Elswick et al., 2007). Because the isotopic fractionation during CO_2 dissolution is approximately 8‰ at 15 °C (McIntosh et al., 2002), the $\delta^{13}C_{DIC}$ should be lighter than −14‰. However, when the SO_4^{2-} concentrations are lower and sulfate reduction is inhibited, methanogenic activity is more pronounced. Due to the larger carbon isotope fractionation during CO_2 reduction to CH_4 and the more negative carbon isotope in microbial methane (<−55‰; Whiticar, 1999), the $\delta^{13}C_{DIC}$ should be much more positive in areas where CO_2 reduction to CH_4 occurred.

The values of $\delta^{13}C$-DIC in this study fall into two groups, −13.9‰ to −8.0‰ and 15.4‰–26.2‰ (Tables 3–6B). The lighter group's $\delta^{13}C$ values decrease with increasing HCO_3^-concentrations. This CO_2

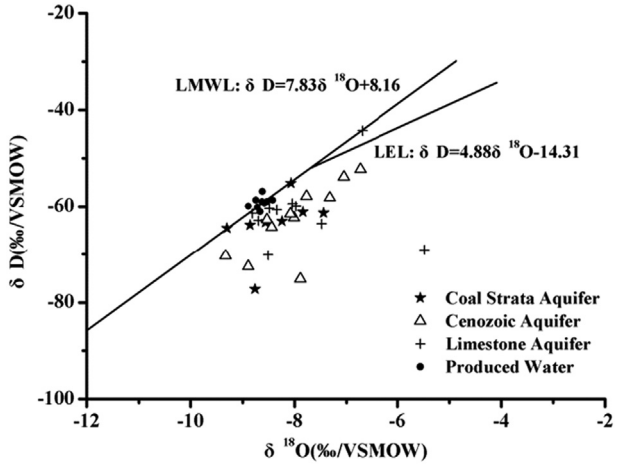

Fig. 7. Relationship of $\delta^{18}O-H_2O$ vs. $\delta D-H_2O$ for produced water, coal strata aquifer, limestone aquifer, and Cenozoic aquifer (LEL is from Chen et al., 2013b).

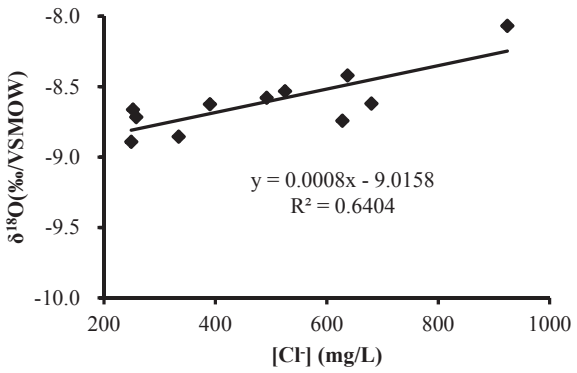

Fig. 8. $\delta^{18}O-H_2O$ vs. $[Cl^-]$of coal strata aquifer according to Table 6.

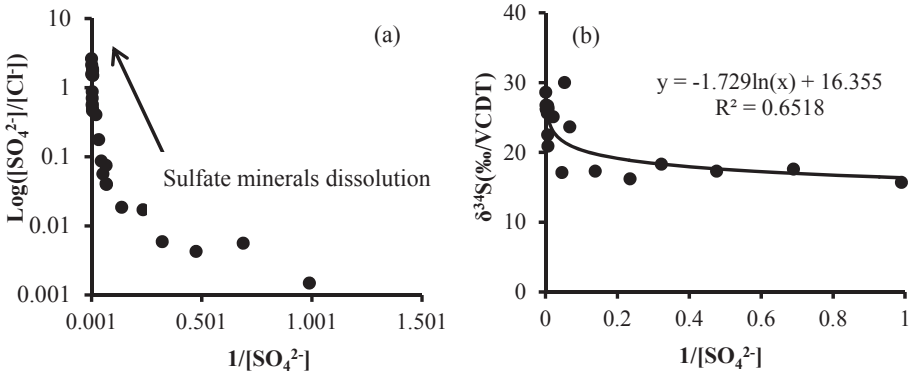

Fig. 9. (a) $[SO_4^{2-}]$ vs. $[Cl^-]$ for the coal strata aquifers and the produced water; (b) $[SO_4^{2-}]$ vs. $\delta^{34}S$–SO_4^{2-} for the coal strata aquifers and the produced water.

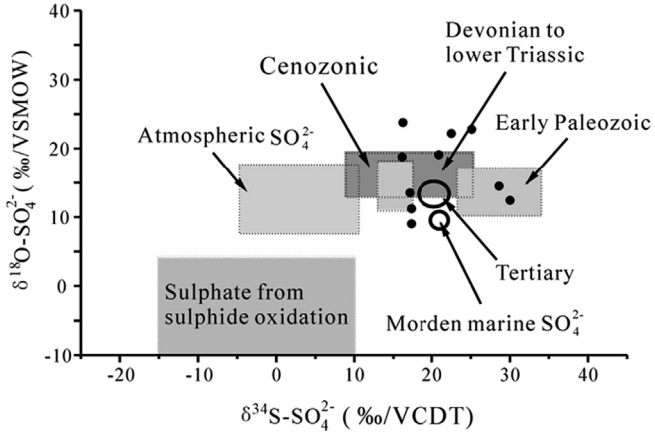

Fig. 10. $\delta^{34}S$ vs. $\delta^{18}O$ for discrimination of different SO_4^{2-} sources (The compositional fields are from Cheung et al., 2010).

might have originated from thermal evolution of the organic matter (Fig. 11a). The heavier group's $\delta^{13}C$ values exhibit a positive correlation with HCO_3^- concentration. Combined with the analysis of water-rock interactions, this correlation is likely to reflect a strong CO_2 reduction reaction (Kinnon et al., 2010). Hence, thermogenic and biogenic origins of CBM are both supported by the evidences from sulfate and DIC isotopes.

The DOC in the formation water could be completely degraded into H_2O and CO_2 by microbes. This process would induce a certain degree of carbon isotope fractionation, and the $\delta^{13}C$ of the remaining DOC would become heavier with the increasing HCO_3^- concentration. So, the microbial activity is confirmed by Fig. 11b. However, the inconspicuous relationship between $\delta^{13}C$-DOC and $\delta^{13}C$-DIC seems to reflect that the biodegradation of DOC should not be an important DIC source. After all, the TOC content is only 1.0 mg/L on average, so its direct biodegradation could not contribute too much for such high DIC levels (>1000 mg/L). In fact, the microbial degradation of organic matter in coal could generate CO_2 in large quantities. Then, CO_2 reduction, a main pathway for biogenic gas generation, should be responsible for the higher $\delta^{13}C$ values of the remaining CO_2 (Whiticar, 1999). As a result, the dissolution of these CO_2 induced $\delta^{13}C_{DIC}$ values exhibiting a positive correlation with HCO_3^- concentration.

According to Table 6B, samples with more positive $\delta^{13}C$-DIC compositions often have higher dissolved gas levels (>700 μl/L). This also supports the idea that the positive $\delta^{13}C$-DIC was caused by CO_2 reduction reaction. More importantly, the concentration of DIC in samples with higher dissolved gas contents are all higher than those with lower dissolved gas contents. However, the SO_4^{2-} concentrations and pH have the opposite relationship with the dissolved gas contents. This is in accordance with previous studies showing that the rapid reproduction of methanogens occurs only in an anoxic environment with appropriate pH ranges and low SO_4^{2-} concentrations (Rice and Claypool, 1981; McIntosh and Martini, 2008; Mitterer, 2010; Schlegel et al., 2011).

Methanogenesis depends on many factors, such as nutrients, dissolved oxygen level, temperature, etc. Though no direct microbiological evidence was presented including the species of the microbes and their abundance in the formation water, extensive methanogen activity and methanogenesis could also be recognized by the hyrogeochemical characteristics analyzed above. However, in order to adequately understand the microbial activity and the

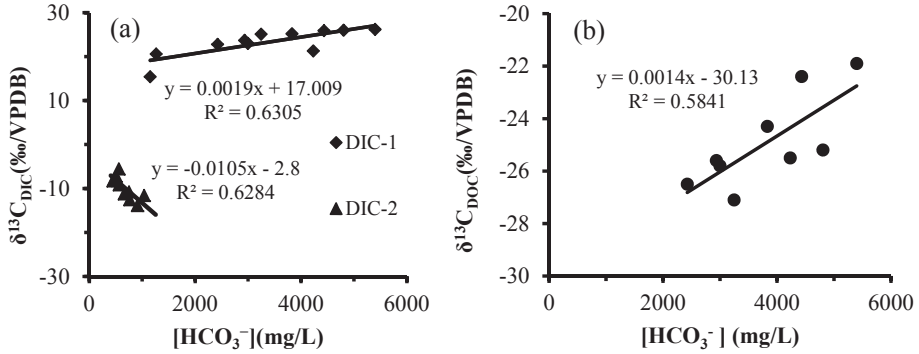

Fig. 11. $[HCO_3^-]$ vs. $\delta^{13}C_{DIC}$ and $[HCO_3^-]$ vs. $\delta^{13}C$-DOC values for the coal strata aquifers (according to Tables 2 and 6B).

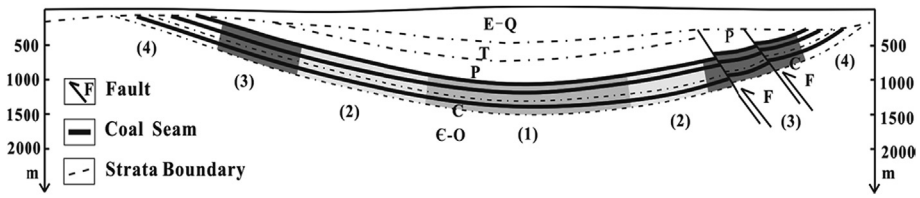

Fig. 12. Occurrence model of gases of different origin in the Huaibei coalfield (modified from Li et al., 2015). (1) Thermogenic gas zone, (2) mixture zone, (3) secondary biogenic gas zone, (4) gas oxidation zone. Є: Cambrian, O: Ordovician; C: Carboniferous; P: Permian; T: Triassic; E: Palaeogene; Q: Quaternary.

forming process of microbial gas, further research about the species of the microbes and other aspects related to the generation of microbial gas is needed.

5.2.4. Microbial methane in coal seams

According to the analysis above and the geochemical characteristics of the gases (Bao et al., 2014; Li et al., 2015), microbial gas was enriched in large quantities in the study area. However, if it had only been generated in the coal strata aquifers, the microbial gas would only be distributed around the formation water instead of in coal seams in large quantities. This enrichment pattern could not form a large enrichment region. Then, another enrichment pattern seems more reasonable: since the Miocene, a relatively enclosed environment favorable for methanogens was formed along with the injection of meteoric water. Some microbes, including methanogens, migrated along with the groundwater and eventually inoculated the coal seams through the structural fractures. In certain areas, the methanogens multiplied rapidly, and a considerable amount of microbial methane was generated (Fig. 12). Then, an enrichment region of secondary biogenic gas was formed, with a mixed zone with thermogenic gas in the lower portion. Another important role of the generation and accumulation of the microbial gas was to prevent the further dissipation of thermogenic gas at the bottom.

According to Strąpoć et al. (2008), the average diameter of methanogens is approximately 0.4 μm. In the study area, the fractures are highly developed with widths mostly greater than 5 μm (Wei, 2014). Hence, the migration of microbes in coal seams is feasible. As a result, biogenic methane could be generated in coal seams via the process of methanogenesis, at a scale depending on the microbial population's size and migration capability.

6. Conclusion

The Cenozoic aquifers have relatively stable and balanced ionic compositions, while the chemical compositions and water quality types of the coal strata and the limestone aquifers are more complex. Ion exchange, calcite precipitation, dissolution of CO_2, and evaporites are the main water-rock interactions in these aquifers. The chemical compositions of the formation water are controlled by varying degrees of evaporite, silicate, and carbonate dissolution. All the aquifers are directly or indirectly recharged by meteoric water. The circumneutral pH and TDS content, positive $\delta^{13}C_{DIC}$ values, lower concentrations of sulfate, and higher concentrations of dissolved methane and DIC are all powerful proofs of extensive methanogenic activity and the idea that microbial methane was generated through the CO_2 reduction pathway. After microbes inoculated the coal seams along with the groundwater infilling the structural fractures, the generation and enrichment of secondary biogenic gas occurred via the process of methanogenesis, at a scale depending on the microbial population's size and migration capability. Overall, the hydrogeochemical characteristics of the aquifers can provide important information for understanding the evolution of the aquifers and recognizing the forming process and occurrence of biogenic gas.

Acknowledgments

This study was funded by the Strategic Priority Research Program "Climate Change: Carbon Budget and Related Issues" of the Chinese Academy of Sciences (XDA05030100), the National Major Research Program for Science and Technology of China (2011ZX05060-005), the National Key Basic Research Program of China (2014CB238901), and the National Natural Science Foundation of China (41530315, 41372213, 41402139). We gratefully appreciate the help from the engineering technicians in the collieries of the study area during sampling.

References

Appelo, C.A.J., Postma, D., 2005. Geochemistry, Groundwater and Pollution, second ed., vol. 201–205. Balkema Rotterdam, The Netherlands, p. 683.
Aravena, R., Harrison, S.M., Barker, J.F., et al., 2003. Origin of methane in the Elk valley coalfield,southeastern British Columbia, Canada. Chem. Geol. 195, 219–227.
Bao, Y., Wei, C.T., Wang, C.Y., et al., 2014. Geochemical characteristics and generation process of mixed biogenic and thermogenic coalbed methane in Luling coalfield, China. Energy & Fuels 28 (7), 4392–4401.
Begley, I.S., Scrimgeour, C.M., 1997. High-precision δ^2H and $\delta^{18}O$ measurement for water and volatile organic compounds by continuous-flow pyrolysis isotope ratio mass spectrometry. Anal. Chem. 69 (8), 1530–1535.
Brenna, J.T., Corso, T.N., Tobias, H.J., Caimi, R.J., 1997. High-precision continuous-flow isotope ratio mass spectrometry. Mass Spectrom. Rev. 16 (5), 227–258.
Brinck, E.L., Drever, J.I., Frost, C.D., 2008. The geochemical evolution of water coproduced with coalbed natural gas in the Powder River Basin, Wyoming. Environ. Geosci. 15, 153–171.
Chapman, J.B., Lewis, B., Greg, L., 2003. Chemical and isotopic evaluation of water sources to the fens of South Park, Colorado. Environ. Geol. 43, 533–545.
Chen, L.W., Yin, X.X., Gui, H.R., et al., 2013a. Water-rock interaction tracing and analysis of deep aquifers in the ming area using isotope and hydrochemistry methods (in Chinese with English abstract). Acta Geol. 87, 1021–1030.
Chen, L.W., Yin, X.X., Chen, Y.P., 2013b. Hydrogen and oxygen stable isotope tracing of deep groundwater Circulation under mining–induced disturbance in mining district (in Chinese with English abstract). Geogr. Geo Inf. Sci. 29, 85–90.
Cheung, K., Klassen, P., Mayer, B., et al., 2010. Major ion and isotope geochemistry of fluids and gases from coalbed methane and shallow groundwater wells in Alberta, Canada. Appl. Geochem. 25, 1307–1329.
Coplen, T.B., 2011. Guidelines and recommended terms for expression of stable-isotope-ratio and gas-ratio measurement results. Rapid Commun. Mass Spectrom. 25 (17), 2538–2560.
Elswick, E.R., Hower, J.C., Carmo, A.M., et al., 2007. Sulfur and carbon isotope geochemistry of coal and derived coal-combustion by-products: an example from an Eastern Kentucky mine and power plant. Int. J. Coal Geol. 22, 2065–2077.
Flores, R.M., Rice, C.A., Stricker, G.D., et al., 2008. Methanogenic pathways of coalbed gas in the Powder River Basin, United States: the geologic factor. Int. J. Coal Geol. 76, 52–75.
Gaillardet, J., Dupré, B., Louvat, P., et al., 1999. Global silicate weathering and CO_2 consumption rates deduced from the chemistry of the large rivers. Chem. Geol. 159, 3–30.
Gao, L., Brassell, S.C., Mastalerz, M., et al., 2013. Microbial degradation of sedimentary organic matter associated with shale gas and coalbed methane in eastern Illinois Basin (Indiana), USA. Int. J. Coal Geol. 107, 152–164.
Golding, S.D., Boreham, C.J., Esterle, J.S., 2013. Stable isotope geochemistry of coal bed and shale gas and related production waters: a review. Int. J. Coal Geol. 120, 24–40.
Gui, H.R., 2005. Study on Hydrogeochemistry Characteristics and Discrimination Pattern of Deep Groundwater in Mining Area of Northern Anhui. University of

Science and Technology of China, Heifei, p. 189.
Hamilton, S.K., Golding, S.D., Baublys, K.A., et al., 2014. Stable isotopic and molecular composition of desorbed coal seam gases from the Walloon Subgroup, eastern Surat Basin, Australia. Int. J. Coal Geol. 122, 21–36.
Han, G.L., Liu, C.Q., 2005. Hydrogeochemistry of rivers in Guizhou Province, China: constraints on crustal weathering in karst terrain (in Chinese with English abstract). Adv. Earth Sci. 20, 394–406.
Healy, R.W., Bartos, T.T., Rice, C.A., et al., 2011. Groundwater chemistry near an impoundment for produced water, Powder River Basin, Wyoming, USA. J. Hydrology 403, 37–48.
Huang, T.M., Pang, Z.H., Edmunds, W.M., 2013. Soil profile evolution following land-use change: implications for groundwater quantity and quality. Hydrol. Process. 27, 1238–1252.
Jiang, B., Qu, Z.H., Wang, G.G.X., et al., 2010. Effects of structural deformation on formation of coalbed methane reservoirs in Huaibei coalfield, China. Int. J. Coal Geol. 82, 175–183.
Ju, Y.W., Li, Q.G., Yan, Z.F., et al., 2014. Origin types of CBM and their geochemical research progress (in Chinese with English abstract). J. China Coal Soc. 39, 806–815.
Kinnon, E.C.P., Golding, S.D., Boreham, C.J., et al., 2010. Stable isotope and water quality analysis of coal bed methane production waters and gases from the Bowen Basin, Australia. Int. J. Coal Geol. 82, 219–231.
Li, Q.G., Ju, Y.W., Bao, Y., et al., 2015. Composition, origin and distribution of CBM in the Huaibei coalfield, China. Energy & Fuels 29, 546–555.
Li, S.Y., Lu, X.X., Bush, R.T., 2014. Chemical weathering and CO_2 consumption in the lower Mekong river. Sci. Total Environ. 472, 162–177.
Martini, A.M., Walter, L.M., Budai, J.M., et al., 1998. Genetic and temporal relations between formation waters and biogenic methane: upper Devonian Antrim Shale, Michigan Basin, U.S.A. Geochim. Cosmochim. Acta 62, 1699–1720.
McIntosh, J.C., Walter, L.M., Martini, A.M., 2002. Pleistocene recharge to mid-continent basins: effects on salinity structure and microbial gas generation. Geochim. Cosmochim. Acta 66, 1681–1700.
McIntosh, J.C., Martini, A.M., 2008. Hydrogeochemical indicators for microbial methane in fractured organic-rich shales: case studies of the Antrim, New Albany, and Ohio Shales. In: Hill, D.G., Lillis, P.G., Curtis, J.B. (Eds.), Gas Shale in the Rocky Mountains and beyond. Rocky Mountain Association of Geologists Guidebook, Denver, pp. 162–174.
Meybeck, M., 1981. Pathways of major elements from land to ocean through rivers. In: Martin, J.M., Burton, J.D., Eisma, D. (Eds.), River Inputs to Ocean Systems. United Nations Press, New York, pp. 18–30.
Mitterer, R.M., 2010. Methanogenesis and sulfate reduction in marine sediments: a new model. Earth Planet. Sci. Lett. 295, 358–366.
Négrel, P., Allègre, C.J., Dupré, B., et al., 1993. Erosion sources determined by inversion of major and trace element ratios and strontium isotopic ratios in river water: the Congo Basin case. Earth Planet. Sci. Lett. 120, 59–76.
Pashin, J.C., McIntyre-Redden, M.R., Mann, S.D., et al., 2014. Relationships between water and gas chemistry in mature coalbed methane reservoirs of the Black Warrior Basin. Int. J. Coal Geol. 126, 92–105.
Rice, C.A., Ellis, M.S., Bullock Jr., J.H., 2000. Water Co-produced with Coal-bed Methane in the Powder River Basin. Preliminary Compositional Data, Wyoming, p. 132. U. S. Geological Survey Open-File Report, 00–372.
Rice, C.A., Flores, R.M., Stricker, G.D., et al., 2008. Chemical and stable isotopic evidence for water/rock interaction and biogenic origin of coalbed methane, Fort Union Formation, Powder River Basin, Wyoming and Montana USA. Int. J. Coal Geol. 76, 76–85.
Rice, D.D., Claypool, G.E., 1981. Generation, accumulation, and resource potential of biogenic gas. AAPG Bull. 65 (1), 5–25.
Schlegel, M.E., McIntosh, J.C., Bates, B.L., et al., 2011. Comparison of fluid geochemistry and microbiology of multiple organic-rich reservoirs in the Illinois Basin, U.S.A.: evidence for controls on methanogenesis and microbial transport. Int. J. Coal Geol. 75 (7), 1903–1919.
Scott, A.R., Kaiser, W.R., Ayers, W.B., 1994. Thermogenic and secondary biogenic gases, San Juan Basin, Colorado and New Mexico-Implications for coalbed gas producibility. AAPG Bull. 78 (8), 1186–1209.
Shuai, Y.H., Zhang, S.C., Grasby, S.E., et al., 2013. Controls on biogenic gas formation in the Qaidam Basin, northwestern China. Chem. Geol. 335, 36–47.
Stueber, A.M., Walter, L.M., 1994. Glacial recharge and paleohydrologic flow systems in the Illinois Basin: evidence from chemistry of Ordovician carbonate (Galena) formation waters. GSA Bull. 106, 1430–1439.
Strąpoć, D., Mastalerz, M., Schimmelmann, A., et al., 2008. Variability of geochemical properties in a microbially dominated coalbed gas system from the eastern margin of the Illinois Basin, USA. Int. J. Coal Geol. 76, 98–110.
Van Voast, W.A., 2003. Geochemical signature of formation waters associated with coalbed methane. AAPG Bull. 87, 667–676.
Warwick, P.D., Breland, F.C., Hackley, P.C., 2008. Biogenic origin of coalbed gas in the northern Gulf of Mexico Coastal Plain, USA. Int. J. Coal Geol. 76, 119–137.
Weaver, T.R., Frape, S.K., Cherry, J.A., 1995. Recentcrossformational fluid flow and mixing in the shallow Michigan Basin. GSA Bull. 107, 697–707.
Wei, M.M., 2014. Research on formation mechanism of CBM enrichment zones and its enrichment models of medium-high rank Coals-a case study of the south of Qinshui basin and Huaibei coalfield, Beijing. Univ. Chin. Acad. Sci. 36–39, 198.
Whiticar, M.J., Faber, E., Schoell, M., 1986. Biogenic methane formation in marine and fresh water environment: CO_2 reduction vs. acetate fermentation–Isotopic evidence. Geochim. Cosmochim. Acta 50 (5), 693–709.
Whiticar, M.J., 1999. Carbon and hydrogen isotope systematics of bacterial formation and oxidation of methane. Chem. Geol. 161, 291–314.
Wu, J.G., Li, W., 2005. Discussion on Technology for drainage and utilization of CBM in Huaibei mining area (in Chinese with English abstract). China Coalbed Methane 2 (4), 16–19.
Wu, Y.D., Ju, Y.W., Hou, Q.L., et al., 2011. Comparison of coalbed gas generation between Huaibei-Huainan coalfields and Qinshui coal basin based on the tectono-thermal modeling. Sci. China Earth Sci. 54 (7), 1069–1077.
Xu, Z.F., Liu, C.Q., 2010. Water geochemistry of the Xijiang basin rivers, South China: chemical weathering and CO_2 consumption. Appl. Geochem. 25, 1603–1614.
Yang, M., Ju, Y.W., Tong, L., et al., 2011. Characteristics of coalbed produced water in the process of coalbed methane development. Environ. Eng. Manag. J. 10, 985–993.
Yang, Y.C., Shen, Z.L., Wen, D.G., et al., 2008. Hydrochemical characteristics and sources of sulfate in groundwater of the ordos Cretaceous groundwater basin (in Chinese with English abstract). Acta Geol. Sin. 29 (5), 553–562.
Zinder, S.H., 1993. Physiological ecology of methanogens. In: Ferry, J.G. (Ed.), Methanogenesis: Ecology, Physiology, Biochemistry and Genetic, vol. 128–206. Chapman and Hall, New York, p. 563.
Zhang, S.C., Shuai, Y.H., Huang, L., et al., 2013. Timing of biogenic gas formation in the eastern Qaidam Basin, NW China. Chem. Geol. 352, 70–80.
Zhang, Y., Gable, C.W., Zyvoloski, G.A., et al., 2009. Hydrogeochemistry and gas compositions of the Uinta Basin: a regional-scale overview. AAPG Bull. 93 (8), 1087–1118.
Zheng, L.G., Liu, G.J., Qi, C.C., et al., 2008. The use of sequential extraction to determine the distribution and modes of occurrence of mercury in Permian Huaibei coal, Anhui Province, China. Int. J. Coal Geol. 73, 139–155.